

Digital Transmitter Coil for Wireless Power Transfer Robust Against Variation of Distance and Lateral Misalignment

Hao Qiu¹, *Member, IEEE*, Takayasu Sakurai, *Fellow, IEEE*, and Makoto Takamiya², *Senior Member, IEEE*

Abstract—A digital transmitter (TX) coil consisting of several subcoils connected in parallel is proposed in wireless power transfer (WPT) systems robust against the variation of distance and lateral misalignment. According to the position of the receiver coil, the radius of the digital TX coil can be programmed to its optimal value to achieve the maximum coil-to-coil efficiency. Moreover, targeting the wireless charging of mobile devices, we propose a practical design methodology for the digital TX coil. It is concluded that the digital TX coil consisting of two subcoils is an effective design and that the performance is not significantly improved by adding more subcoils. The optimal radius ratio of these two subcoils is 0.54. Furthermore, we implement the designed digital TX coil in a prototype WPT system, including a power amplifier and a rectifier. Experimental results show that within a space with a maximum distance and lateral misalignment of 100 mm, the system efficiency is improved by the digital TX coil and reaches a maximum value of 48%. Compared with using a conventional TX coil with a constant radius, the system efficiency shows an absolute improvement of up to 7%.

Index Terms—Coil design methodology, coil-to-coil efficiency, distance, lateral misalignment, magnetic resonance coupling, mutual inductance, optimal radius, wireless power transfer (WPT).

I. INTRODUCTION

WIRELESS power transfer (WPT) based on magnetic resonance coupling has been applied in a wide range of applications, such as mobile devices and biomedical implanted devices [1]–[3]. The variation of the distance and lateral misalignment of the receiver (RX) coil relative to the transmitter (TX) coil, however, strongly affects the WPT system efficiency (η_{SYS}) and is a critical problem. The discussion of angular misalignment is out of the scope of this article. During the wireless charging of mobile devices, it is preferable that devices are not placed on a wireless charging pad but can be held in hand and operated. Therefore, a method robust against the variation of distance and lateral misalignment is required for WPT systems.

Manuscript received January 11, 2020; revised March 9, 2020; accepted April 12, 2020. Date of publication May 14, 2020; date of current version September 2, 2020. This work was supported by Japan Science and Technology Agency (JST) Exploratory Research for Advanced Technology (ERATO), Japan, under Grant JPMJER1501. (*Corresponding author: Hao Qiu.*)

The authors are with the Institute of Industrial Science, The University of Tokyo, Tokyo 153-8505, Japan (e-mail: hqiu@iis.u-tokyo.ac.jp).

Color versions of one or more of the figures in this article are available online at <http://ieeexplore.ieee.org>.

Digital Object Identifier 10.1109/TMTT.2020.2990976

The previously reported methods are mainly divided into three categories [1]: control methods [4]–[11], circuit compensation topologies [12]–[14], and coil design [15]–[18]. In the first category, frequency tracking [4]–[6], impedance matching networks [7], [8], and coil repeaters [9]–[11] have been proposed to achieve impedance matching between the TX coil input impedance and the source impedance over a wide range. In the second category, in addition to the traditional compensation topologies (series–series, series–parallel, parallel–series, and parallel–parallel), several new topologies, such as capacitor–capacitor–inductor [12], inductor–capacitor–capacitor [13], and hybrid topologies [14], with better misalignment performance have been proposed. However, in the above-mentioned two categories, the complex circuit topology makes the system more sensitive to parameter variations [19], affecting its reliability. In addition, coil-to-coil efficiency (η) cannot be improved.

On the other hand, in the third category, the coil design can directly maximize η , and thus, maximize η_{SYS} . From the practical viewpoint, the TX coil design is preferable to the RX coil design. In [15], the pattern of the TX coil was designed to realize a relatively uniform magnetic field distribution under lateral misalignment. However, its tolerance to the variation of distance is not demonstrated. In [16], the optimal TX coil layout design with respect to the distance was proposed, but it was not discussed how to change its layout adaptively. Volumetric coil structures [17], [18] have been proposed to minimize the effects of variation of distance and lateral misalignment but are not easily implementable in practice.

Our major contributions in this article are summarized as follows: 1) we propose a digital TX coil topology, which consists of several subcoils connected in parallel where the coil radius can be programmed to its optimal value giving the maximum η . 2) We propose a practical design methodology for the digital TX coil, including the number of subcoils and their radii, under the variation of distance and lateral misalignment. 3) We implement the digital TX coil in a prototype and demonstrate its effectiveness in a WPT system robust against the variation of distance and lateral misalignment. Compared with our earlier work [20], we have added a discussion about lateral alignment, proposed a practical design methodology, and implemented the digital TX coil in a prototype WPT system.

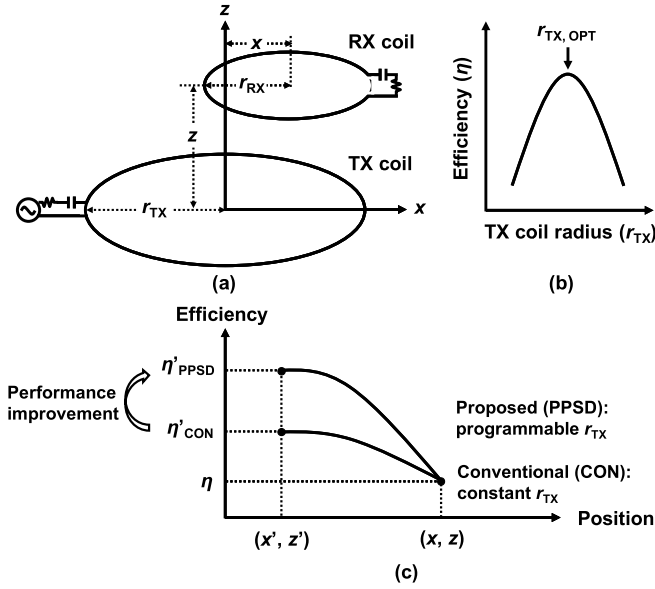


Fig. 1. (a) Configuration of the TX and RX coils. A single turn of TX and RX coils is shown for simplicity. (b) r_{TX} dependence of η . (c) Position dependence of η using the conventional TX coil with constant r_{TX} and the proposed TX coil with programmable r_{TX} .

The rest of this article is organized as follows. In Section II, the optimal radius of the TX coil giving the maximum η is discussed. Then, the digital TX coil topology is proposed in Section III. A practical design methodology for the digital TX coil under the variation of distance and lateral misalignment is proposed in Section IV. Experimental results are presented in Section V. Finally, conclusions are given in Section VI.

II. OPTIMAL TRANSMITTER COIL RADIUS FOR MAXIMUM EFFICIENCY UNDER THE VARIATION OF DISTANCE AND LATERAL MISALIGNMENT

Fig. 1 shows the key concept of this article. The configuration of the TX and RX coils is shown in Fig. 1(a). The radii of the TX and RX coils are denoted by r_{TX} and r_{RX} , respectively. In this article, the axes of the coils are always parallel. Distance and lateral misalignment are denoted by z and x , respectively. As shown in Fig. 1(b), η shows a peak when r_{TX} approaches its optimized value ($r_{TX,OPT}$) and a smaller or larger r_{TX} will degrade η [20], [21]. In our WPT system design, we first optimize the TX coil to maximize η at the farthest position (x, z). When the RX coil moves nearer to (x', z') , with a constant r_{TX} in the conventional (CON) design, η increases to η^{CON} owing to the enhanced coupling. On the other hand, if a TX coil with an adjustable r_{TX} is used in the proposed (PPSD) design, η^{CON} can be further improved to η^{PPSD} . Thus, compared with the conventional design, the proposed design can achieve better misalignment tolerance. In this section, we derive the relationship between $r_{TX,OPT}$ and (x, z) .

A. Equivalent Circuit Analysis

Fig. 2 shows the equivalent circuit of a WPT system. The TX side consists of a voltage source (V_S) with an internal

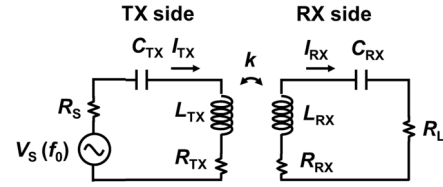


Fig. 2. Simplified equivalent circuit of a WPT system.

resistance (R_S), an inductor (L_{TX}) with a parasitic resistance (R_{TX}), and a compensation capacitor (C_{TX}). The RX side is composed of an inductor (L_{RX}) with a parasitic resistance (R_{RX}), a compensation capacitor (C_{RX}), and a load resistance (R_L). The currents flowing in the TX and RX sides are I_{TX} and I_{RX} , respectively. k is the coupling coefficient between the TX and RX coils. Applying Kirchhoff's voltage law to the circuit, we obtain the following equations at the resonance frequency (f_0):

$$\omega_0 = 2\pi f_0$$

$$M = k\sqrt{L_{TX}L_{RX}}$$

$$V_S = I_{TX}[R_S + R_{TX} + j\omega_0 L_{TX} + 1/(j\omega_0 C_{TX})] - j\omega_0 M I_{RX}$$

$$j\omega_0 M I_{TX} = I_{RX}[R_L + R_{RX} + j\omega_0 L_{RX} + 1/(j\omega_0 C_{RX})]$$

$$L_{TX}C_{TX} = L_{RX}C_{RX} = (\omega_0)^{-2} \quad (1)$$

where M is the mutual inductance between the TX and RX coils, ω_0 is the resonant angular frequency, and j is the imaginary unit.

η is defined by the ratio of the power output from the RX coil to the power input into the TX coil [22]. In addition, when R_L is assumed to equal its optimal value ($R_{L,OPT}$) of $R_{RX} (1 + k^2 Q_{TX} Q_{RX})^{1/2}$, η can be expressed as

$$\eta = \frac{k^2 Q_{TX} Q_{RX}}{(1 + \sqrt{1 + k^2 Q_{TX} Q_{RX}})^2} \quad (2)$$

where

$$k^2 Q_{TX} Q_{RX} = \frac{(\omega_0 M)^2}{R_{TX} R_{RX}} \quad (3)$$

Here, Q_{TX} and Q_{RX} are the quality factors of the TX and RX coils, respectively. Thus, η can be maximized by maximizing $k^2 Q_{TX} Q_{RX}$.

B. Derivation of Optimal Transmitter Coil Radius

$k^2 Q_{TX} Q_{RX}$, on the other hand, is correlated with the physical parameters of the coils. First, we discuss the calculation of the coil resistances. For a tightly wound coil, the resistance depends on both the skin effect and the proximity effect and can be expressed as follows [23]:

$$R_{TX} = \frac{2mr_{TX}}{\sigma \omega^2} \left(1 + \frac{\omega}{\delta} + \frac{3\delta}{4\omega}\right) (1 + G_p) \quad (4)$$

$$R_{RX} = \frac{2nr_{RX}}{\sigma \omega^2} \left(1 + \frac{\omega}{\delta} + \frac{3\delta}{4\omega}\right) (1 + G_p). \quad (5)$$

Here, σ is the conductivity of copper (5.96×10^7 S/m), and ω is the diameter of the copper wire (1 mm). m and n are

the numbers of turns of the TX and RX coils, respectively. The skin depth (δ) is calculated as $(\pi \mu_0 f_0 \sigma)^{-1/2}$, where μ_0 is the vacuum permeability ($4\pi \times 10^{-7}$ H/m). The proximity effect is included in the proximity factor (G_p) [24].

Second, employing Neumann's equation [25], M can be determined by adding all combinations of M_{pq} between the p loop of the TX coil and the q loop of the RX coil

$$M = \sum_{p=1}^m \sum_{q=1}^n M_{pq}$$

and

$$M_{pq} = \frac{\mu_0}{\pi} \sqrt{r_{TX} r_{RX}} \int_0^\pi \frac{\left(1 - \frac{x}{r_{RX}} \cos \phi\right) \Phi(\beta)}{\sqrt{U^3}} d\phi \quad (6)$$

where

$$U = \sqrt{1 + \frac{x^2}{r_{RX}^2} - 2 \frac{x}{r_{RX}} \cos \phi} \quad (7)$$

$$\Phi(\beta) = \left(\frac{2}{\beta} - \beta\right) K(\beta) - \frac{2}{k} E(\beta) \quad (8)$$

$$\beta = \sqrt{\frac{4r_{TX}r_{RX}U}{(r_{RX} + r_{TX}U)^2 + z_{pq}^2}} \quad (9)$$

$$z_{pq} = z + \frac{p-1}{m} t_{TX} + \frac{q-1}{n} t_{RX}. \quad (10)$$

Here, ϕ is the angle in the integration, and K and E are the first kind and the second kind of complete elliptic integrals, respectively [26]. t_{TX} and t_{RX} are the thicknesses of the TX and RX coils, respectively. z_{pq} denotes the distance of the q loop of the RX coil relative to the p loop of the TX coil, and z is defined as z_{pq} when $p = q = 1$.

Thus, by substituting (4)–(6) into (3), $k^2 Q_{TX} Q_{RX}$ can be obtained. It is found that when f_0 , m , n , and r_{RX} are constants, for a specific (x, z) , $k^2 Q_{TX} Q_{RX}$ reaches its maximum when r_{TX} equals $r_{TX,OPT}$, which is obtained by solving

$$\frac{\partial}{\partial r_{TX}} k^2 Q_{TX} Q_{RX} = 0. \quad (11)$$

In this article, we consider our target application as wireless charging of mobile devices and select f_0 as 150 kHz. The maximum z (z_{max}) and maximum x (x_{max}) are both set as 100 mm. Fig. 3(a) shows the calculated dependence of $r_{TX,OPT}$ on (x, z) obtained from (11) using $r_{RX} = 100$ mm, $m = n = 10$, and $t_{TX} = t_{RX} = 13$ mm. Starting from $r_{TX,OPT} = 100$ mm at (0 mm, 0 mm), $r_{TX,OPT}$ increases with increasing misalignment and reaches 205 mm at (100 mm, 100 mm). Fig. 3(b) shows the coil configurations at four selected positions (A, B, C, and D). Compared with the distance dependence, $r_{TX,OPT}$ is affected more strongly by lateral misalignment.

III. PROPOSED DIGITAL TRANSMITTER COIL TOPOLOGY

To implement the TX coil with a programmable r_{TX} according to different positions of the RX coil, a digital TX coil topology is proposed. Fig. 4 shows a schematic of the WPT system. The TX side consists of a power amplifier (PA), the proposed digital TX coil, and a switch (SW) control

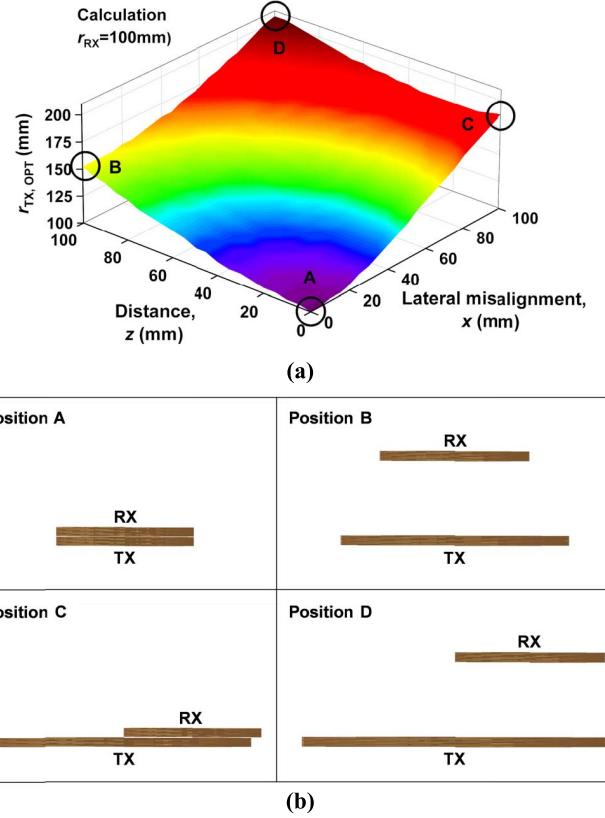


Fig. 3. (a) $r_{TX,OPT}$ surface under different misalignment conditions. Both z_{max} and x_{max} equal 100 mm. The x and z axes are reversed to clearly show the data. (b) Coil configurations under four misalignment conditions.

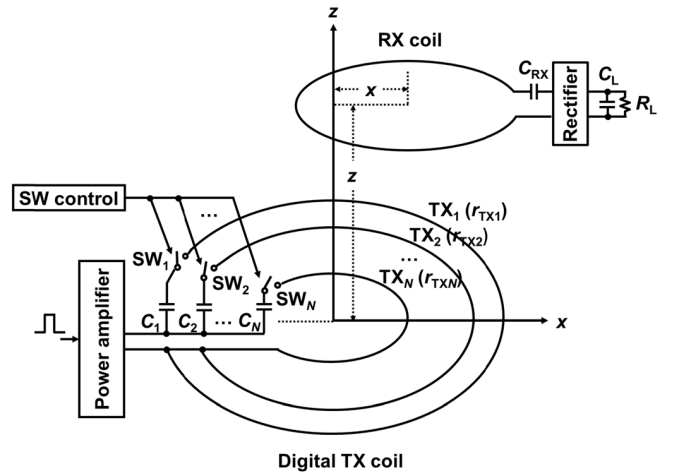


Fig. 4. Schematic of the WPT system in which a PA, the proposed digital TX coil, the RX coil, and a rectifier are implemented. A single turn of TX and RX coils is shown for simplicity.

unit. The digital TX coil consists of N concentric subcoils connected in parallel. The l coil (TX_l) with a radius of r_{TXl} is connected with the corresponding compensation capacitance (C_l) and SW (SW_l) in series, where $l = 1, 2, \dots, N$. The RX side consists of the RX coil, a rectifier followed by a smoothing capacitor (C_L), and R_L . For each specific position

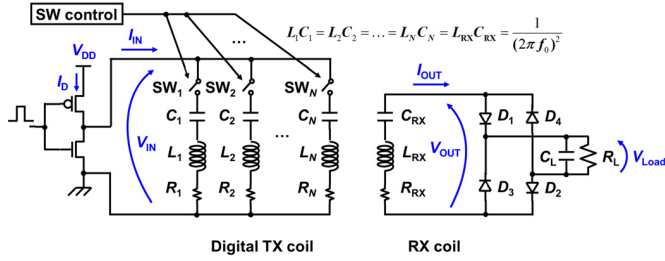


Fig. 5. Equivalent circuit of the WPT system.

of the RX coil, one of the subcoils is turned on. Thus, the radius of the digital TX coil can be adjusted to the corresponding $r_{TX,OPT}$ electronically rather than mechanically, such as by using motors. In addition, a LabVIEW program is developed to support the automatic operation of the SW control unit. Details are given in Section V-A.

Fig. 5 shows the equivalent circuit. The l subcoil in the digital TX coil is denoted by an inductance (L_l) and a parasitic resistance (R_l) connected in series. f_0 for each subcoil in the digital TX coil is the same as that of the RX coil. The rectifier consists of four diodes, D_1 – D_4 . The dc voltage supply is V_{DD} , and the dc current flowing into the PA is I_D . The input voltage and current of the digital TX coil are denoted by V_{IN} and I_{IN} , respectively. The output voltage and current of the RX coil are denoted by V_{OUT} and I_{OUT} , respectively. The voltage across R_L is denoted by V_{Load} .

IV. DESIGN METHODOLOGY OF DIGITAL TRANSMITTER COIL UNDER THE VARIATION OF DISTANCE AND LATERAL MISALIGNMENT

Using the proposed digital TX coil with adjustable r_{TX} , we can obtain the maximum η at each position. However, it would be impractical to implement the digital TX coil with an infinite number of subcoils, considering that in the application scenario, the RX coil can move continuously within the wireless charging space. Thus, in this section, we propose a practical design methodology that determines the number of subcoils in the digital TX coil and their radii ($r_{TX1,OPT}$, $r_{TX2,OPT}$, \dots , $r_{TXN,OPT}$) under the variation of distance and lateral misalignment.

A. Performance Indicator

First, we define the average η ($\bar{\eta}$) as the key performance indicator

$$\bar{\eta} = \frac{\int_0^{x_{\max}} \int_0^{z_{\max}} \eta dz dx}{x_{\max} z_{\max}}. \quad (12)$$

A higher $\bar{\eta}$ indicates a better performance.

B. Design Methodology of Digital Transmitter Coil

In this part, we calculate and compare $\bar{\eta}$ values for different N . As discussed at the beginning of Section II, we first maximize η at (x_{\max}, z_{\max}) and set r_{TX1} as 205 mm in accordance with position D in Fig. 3(b).

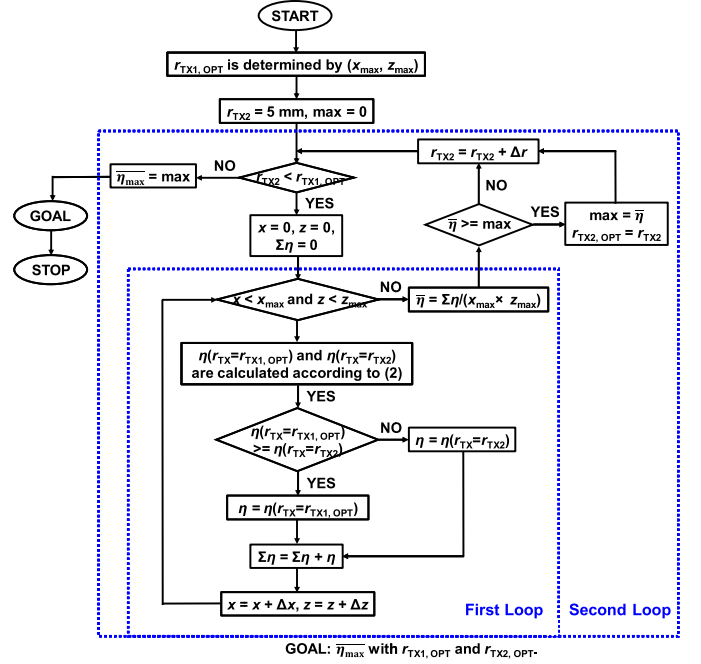


Fig. 6. Flowchart to calculate $r_{TX1,OPT}$, $r_{TX2,OPT}$, and the corresponding $\bar{\eta}_{max}$ for $N = 2$.

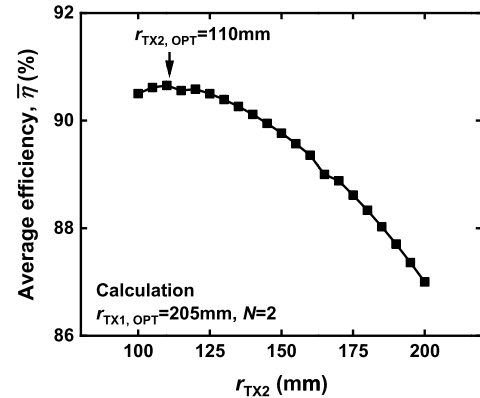


Fig. 7. Calculated r_{TX2} dependence of $\bar{\eta}$ in the case of $N = 2$.

In the case of $N = 1$, which corresponds to TX_1 with $r_{TX1,OPT}$, $\bar{\eta}$ can be easily calculated as 87% using (2), (3), and (12). For $N = 2$, Fig. 6 shows the flowchart to calculate $r_{TX2,OPT}$ and the corresponding maximum $\bar{\eta}$ ($\bar{\eta}_{max}$). Regarding the selection of Δx , Δz , and Δr , there is a tradeoff between calculation accuracy and calculation cost. A smaller size increment gives a more accurate definition of $r_{TX2,OPT}$, but is at the cost of longer calculation time. We set the size increment as 5 mm in our work. There are two calculation loops. In the first loop, $\bar{\eta}$ is calculated for a specific r_{TX2} . For each (x, z) , TX_1 or TX_2 is turned ON, depending on which gives the higher η . After obtaining the η distribution within the range of (x_{\max}, z_{\max}) , $\bar{\eta}$ is calculated using (12). In the second loop, r_{TX2} is changed step by step until $\bar{\eta}_{max}$ is obtained. Fig. 7 shows the r_{TX2} dependence of $\bar{\eta}$. When r_{TX2} equals $r_{TX2,OPT}$, $\bar{\eta}_{max}$ is 91%. Thus, for $N = 2$, $r_{TX1,OPT}$ and

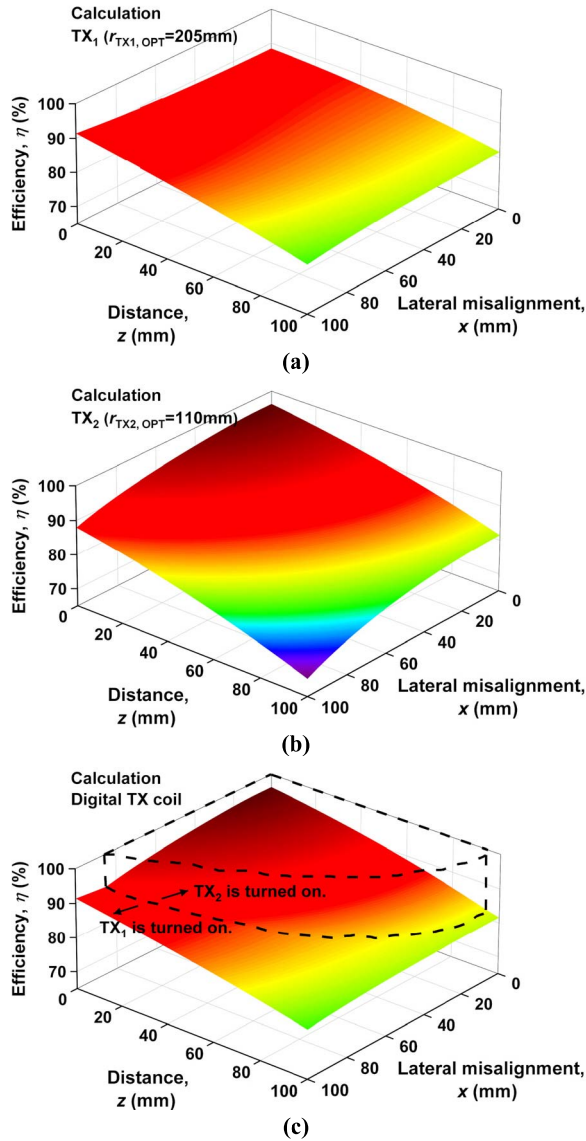


Fig. 8. Calculated η surfaces using (a) TX₁, (b) TX₂, and (c) digital TX coil for $N = 2$ under different misalignment conditions.

$r_{TX2,OPT}$ equal 205 and 110 mm, respectively, and η_{max}^- is greater than that for $N = 1$.

To demonstrate how $\overline{\eta_{max}}$ increases from $N = 1$ to $N = 2$, Fig. 8 shows a comparison of η surfaces using TX₁ with $r_{TX1,OPT}$, TX₂ with $r_{TX2,OPT}$, and the digital TX coil for $N = 2$. TX₁ and TX₂ perform well far from and near (0 mm, 0 mm), respectively. Thus, as shown in Fig. 8(c), with TX₁ and TX₂ turned ON outside and inside the highlighted black volume, respectively, the digital TX coil achieves a higher η than TX₁ in Fig. 8(a). The boundary on the η surface is defined by $\eta(r_{TX} = r_{TX1,OPT}) = \eta(r_{TX} = r_{TX2,OPT})$.

After obtaining $\overline{\eta_{max}}$ for $N = 1$ and 2, the results for $N = 3-6$ are calculated and are shown in Fig. 9(a). It is found that $\overline{\eta_{max}}$ is improved greatly by using two subcoils but increases slightly when N exceeds two. This means that the digital TX coil consisting of two subcoils is a practical design,

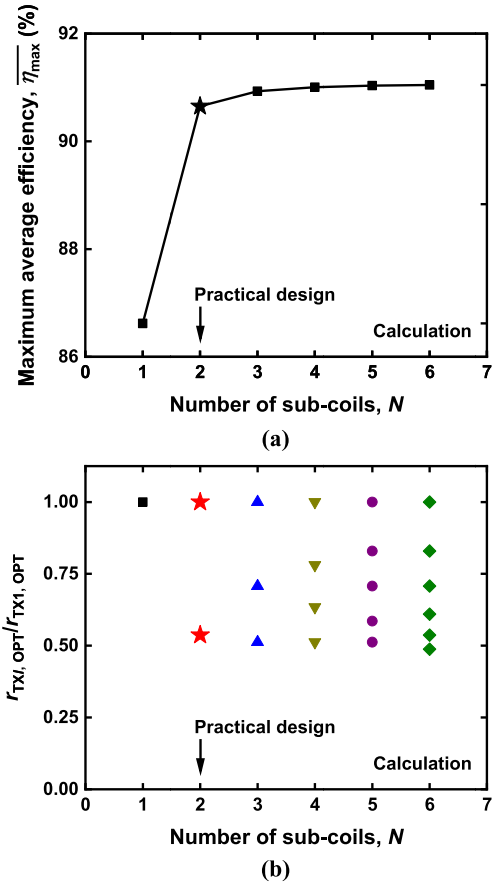


Fig. 9. Calculated N dependence of (a) $\overline{\eta_{max}}$ and (b) ratio of $r_{TXl,OPT}$ to $r_{TX1,OPT}$, where $l = 1, 2, \dots, N$.

and adding any more subcoils only increases the system's cost without significantly improving its performance. Fig. 9(b) shows the ratio of $r_{TXl,OPT}$ ($l = 1, 2, \dots, N$) to $r_{TX1,OPT}$ for different N . In the optimized design ($N = 2$), the ratio of $r_{TX2,OPT}$ to $r_{TX1,OPT}$ is 0.54.

When using the digital TX coil with the optimized design, η_{max}^- is 91%, compared with 87% obtained using the conventional TX design, that is, $N = 1$. In this article, the coil parameters are selected to obtain high-quality factors, and the possible improvement of the performance is limited. Thus, in real applications where the coil quality factors are usually lower, the advantage of using the proposed digital TX coil over the conventional TX coil will be greater.

C. Scalability of Proposed Design Methodology

In addition, the scalability of the proposed design methodology is discussed. It has been demonstrated that the ratio of the distance to the coil radius determines η in a WPT system [27], [28]. Then, it can be predicted that, under the variation of distance and lateral misalignment, η is determined by the ratios of the distance and lateral misalignment with the coil radius. Thus, if the WPT system is scaled up or down with constant ratios of x_{max}/r_{RX} and z_{max}/r_{RX} , the same results as in Fig. 9 can be obtained (data not shown). This indicates that

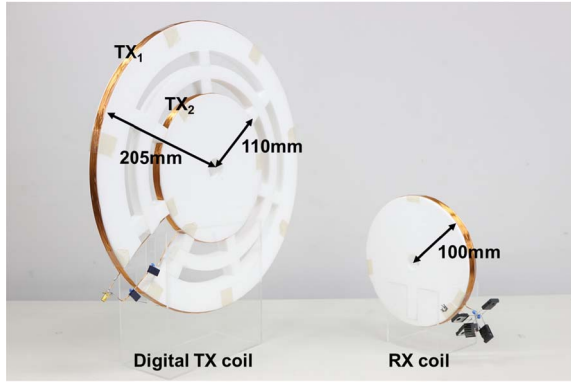


Fig. 10. Photograph of the digital TX coil consisting of TX₁ and TX₂ with the optimized design and the RX coil.

TABLE I
MEASURED PHYSICAL AND ELECTRICAL PARAMETERS
OF DIGITAL TX COIL AND RX COIL

DIGITAL TRANSMITTER COIL		RECEIVER COIL	
Parameter	Value	Parameter	Value
r_{TX1}	205 mm	r_{RX}	100 mm
t_{TX1}	13 mm	t_{RX}	13 mm
m_1	10	n	10
f_0	150 kHz	f_0	150 kHz
L_1	110 μ H	L_{RX}	44.0 μ H
C_1	10.2 nF	C_{RX}	25.6 nF
R_1	0.80 Ω	R_{RX}	0.43 Ω
Q_1	129	Q_{RX}	96
r_{TX2}	110 mm	C_L	6.8 μ F
t_{TX2}	13 mm	R_L	10 Ω
m_2	10		
L_2	48.3 μ H		
C_2	23.3 nF		
R_2	0.50 Ω		
Q_2	91		

t_{TX1} and t_{TX2} are the thicknesses of TX₁ and TX₂, respectively. m_1 and m_2 are the numbers of turns of TX₁ and TX₂, respectively.

our proposed design methodology is universal and independent of the system size.

V. EXPERIMENTAL RESULTS

To verify the effectiveness of the designed digital TX coil in a WPT system robust against the variation of distance and lateral misalignment, we implement the digital TX coil in a prototype WPT system, including a PA and a rectifier. The experimental results are compared with the calculation results.

A. Prototype WPT System Utilizing Digital Transmitter Coil

Fig. 10 shows a photograph of the digital TX coil consisting of TX₁ and TX₂ with the practical design in Section IV. All coils are made of 18 AWG (RS Pro) wire. Table I shows their physical dimensions and electrical parameters measured using a network analyzer (Keysight E5061B). Relays (Panasonic TQ2-L2-4.5) with an ON-resistance of less than 50 m Ω are used as the SWs.

As is shown in Fig. 11, a signal generator (Tektronix AFG3252) is used to generate a square wave signal at 150 kHz

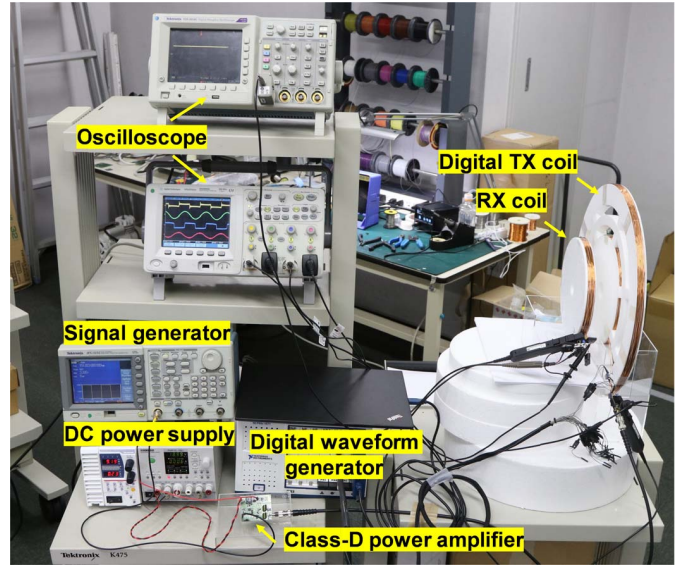


Fig. 11. Photograph of the WPT prototype consisting of a PA, the digital TX coil, the RX coil, and a rectifier with a dc load.

to drive a class-D PA (EPC 9511) [29]. The power of the class-D PA is supplied by TAKASAGO ZX-S-400LAN and KIKUSUI PMP16-1QU. The PA supplies the power to the digital TX coil, which is then wirelessly transferred to the RX coil. The four diodes in the rectifier use a DSEP60-12A Schottky diode from IXYS Corporation, Milpitas, CA, USA, C_L and R_L are an FG22 \times 7.1H685KRT06 capacitor (6.8 μ F) from TDK Corporation, Tokyo, Japan, and a PF2205-10RF1 resistor (10 Ω) from Riedon Resistors, Inc., Alhambra, CA, USA, respectively. For each position of the RX coil, SW₁ and SW₂ are turned ON one by one, and the corresponding V_{DD} , I_D , V_{IN} , I_{IN} , V_{OUT} , I_{OUT} , and V_{Load} (shown in Fig. 5) are monitored using voltage probes (Tektronix P6139B) and current probes (Tektronix P6021A). The results are shown on oscilloscopes (Agilent D5054A and Tektronix TDS3054C). By measuring V_{IN} , I_{IN} , V_{OUT} , and I_{OUT} , we can calculate η .

η_{SYS} is defined as the power delivered to R_L divided by the dc power supply and is expressed as

$$\eta_{SYS} = \frac{V_{Load}^2/R_L}{V_{DD}I_D} \quad (13)$$

where the digital control power in the class-D PA is also included.

A LabVIEW control program is then run on a computer to process the information and generate the control voltages for SW₁ and SW₂ through a digital waveform generator (National Instruments PXIe-6555). η_{SYS} is selected as the criterion for subcoil selection. If η_{SYS} using TX₁ is higher than that using TX₂, SW₁ is turned ON. Otherwise, SW₂ is turned ON. Another possible criterion is η , which would make the implementation more feasible. By measuring k between each subcoil and the RX coil, $k^2 Q_{TX} Q_{RX}$ and η can be simply calculated. In addition, k can be obtained by simply monitoring V_{IN} and I_{IN} [22], [30], without using a directional coupler or a network analyzer to measure S parameters, such as in other

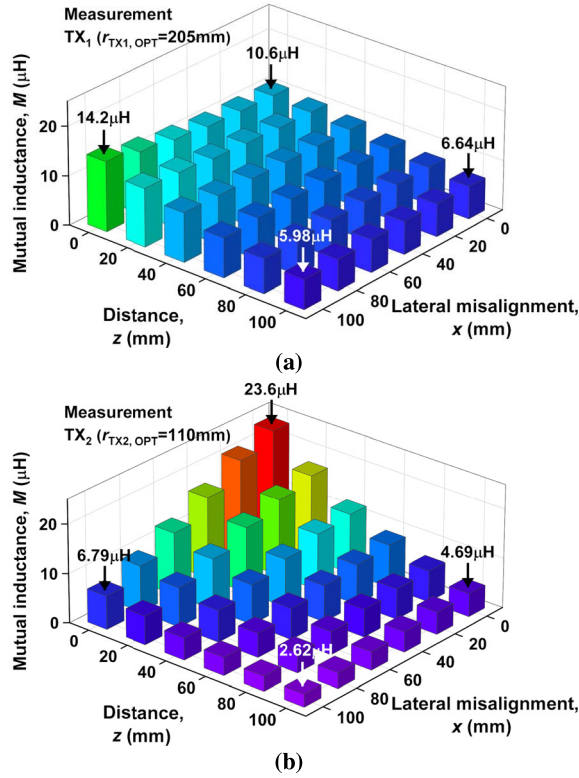


Fig. 12. Measured M using (a) TX₁ and (b) TX₂ under different misalignment conditions.

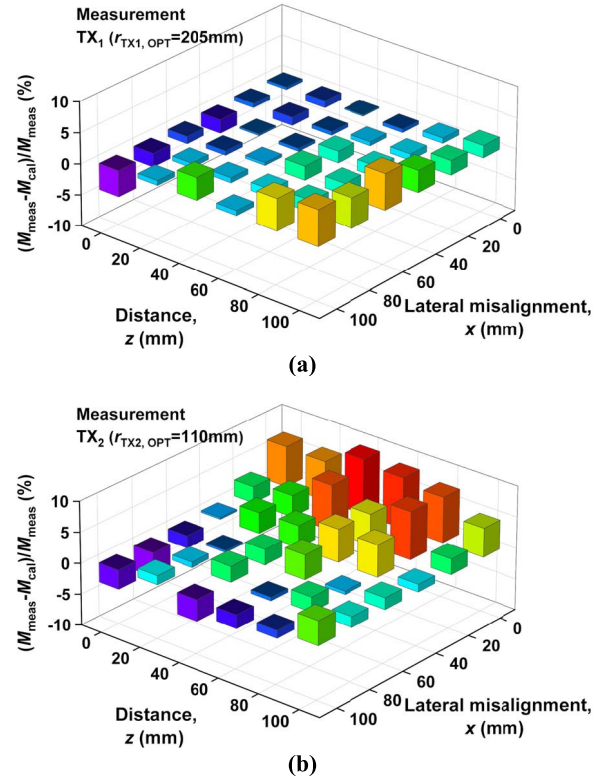


Fig. 13. Error between calculated M and measured M using (a) TX₁ and (b) TX₂ under different misalignment conditions.

systems [5], [7], [11]. Thus, a simple switch control is realized. These two criteria will be compared in Section V-C.

B. Measurement and Comparison of Mutual Inductance

To confirm the accuracy of the calculation results, M is measured in 2-D along the x - and z -directions every 20 mm from 0 to 100 mm using the method described in [22].

Fig. 12(a) shows the measured M (M_{meas}) between TX₁ and the RX coil. Starting from 10.6 μH at (0 mm, 0 mm), M_{meas} drops to 6.64 μH at (0 mm, 100 mm), which is a 37% reduction. On the other hand, it rises to 14.2 μH at (100 mm, 0 mm), a 33% increase, which is ascribed to the asymmetrical radii between TX₁ and the RX coil [21]. When the position of the RX coil is changed to (100 mm, 100 mm) with the largest misalignment, M_{meas} drops to 5.98 μH , which is a 44% reduction. Fig. 12(b) shows M_{meas} between TX₂ and the RX coil. M_{meas} shows a maximum of 23.6 μH at (0 mm, 0 mm) and reductions of 80%, 71%, and 89% at (0 mm, 100 mm), (100 mm, 0 mm), and (100 mm, 100 mm), respectively.

Fig. 13(a) and (b) shows a comparison of M_{meas} and the calculated M (M_{cal}). The error is defined as $(M_{\text{meas}} - M_{\text{cal}})/M_{\text{meas}}$ and shows different trends for TX₁ and TX₂. It is small for TX₁ but large for TX₂ when the RX coil is near (0 mm, 0 mm). However, in both cases, the error is less than 10% over the entire region, which demonstrates the accuracy of (6) in calculating M . In addition, compared with the measurement results, the calculated R_{TX} and R_{RX} using (4) and (5) also show an error within 10% (data not shown). All these results

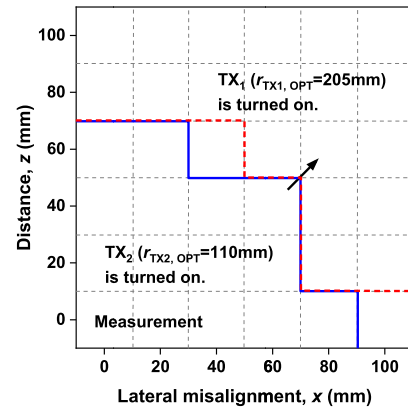


Fig. 14. Measured distribution map showing where TX₁ or TX₂ in the digital TX coil is turned ON. When the RX coil is near (0 mm, 0 mm), TX₂ is turned ON. Otherwise, TX₁ is turned ON. There are two boundaries. One is a blue solid line determined by whether TX₁ or TX₂ achieves the higher system efficiency. The other one is a red dashed line determined by which whether TX₁ or TX₂ achieves the higher coil-to-coil efficiency.

verify the accuracy of the calculation results and validate the proposed design methodology of the digital TX coil.

C. System Efficiency Measurement of WPT Prototype

To evaluate the performance of the WPT prototype, starting from (0 mm, 0 mm), η_{SYS} is measured point by point in 2-D along the x - and z -directions every 20 mm from 0 to 100 mm. At each position, the power supply of the class-D PA is modulated to regulate the power delivered to R_L to 0.9 W.

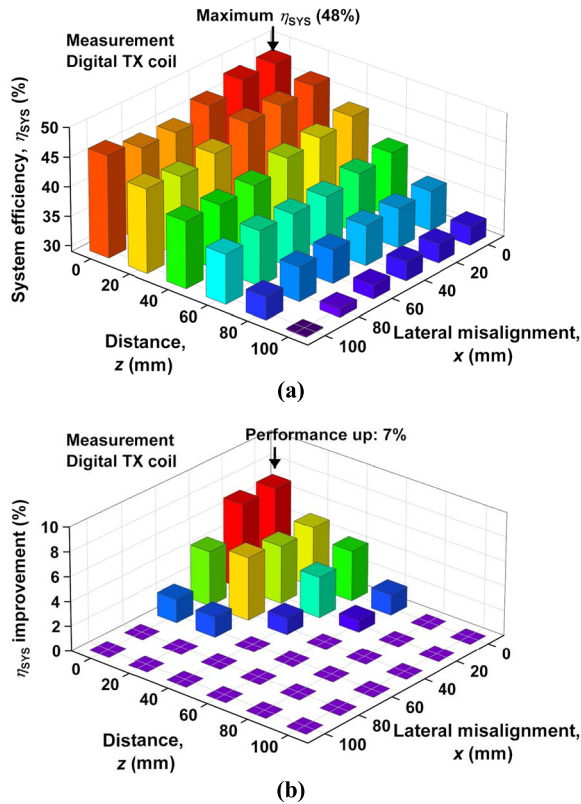


Fig. 15. (a) Measured η_{SYS} using the digital TX coil under different misalignment conditions. (b) Improvement in measured η_{SYS} using the digital TX coil compared with the conventional TX coil (TX_1) under different misalignment conditions.

Depending on which coil achieves the higher η_{SYS} , TX_1 or TX_2 in the digital TX coil is turned ON automatically, as described in Section V-A. In the measured distribution map shown in Fig. 14, the boundary indicated by the blue solid line distinguishes the regions where TX_1 or TX_2 is turned ON. When the RX coil is near (0 mm, 0 mm), TX_2 is turned ON. Otherwise, TX_1 is turned ON.

In addition, the distribution map using η rather than η_{SYS} as the criterion is shown for comparison in Fig. 14. The boundary is indicated by the red dashed line. This line coincides with the blue solid line except at two positions. Take the black arrow as an example. The switching from TX_2 to TX_1 increases η . From a systematic viewpoint, a different TX coil results in a different k , which will change the reflected impedance from the RX coil, and thus, affect η_{SYS} . However, η_{SYS} is still increased. Thus, it can be concluded that η plays an important role in determining η_{SYS} , as mentioned in Section I.

Fig. 15(a) shows the measured η_{SYS} using the digital TX coil. It has a maximum value of 48% at (0 mm, 0 mm). In Fig. 15(b), η_{SYS} is shown to be improved under the variation of distance and lateral misalignment compared with that for the conventional TX coil (TX_1). The maximum absolute improvement of 7% is at (0 mm, 0 mm), which is the most common position of the RX coil.

VI. CONCLUSION

A WPT system utilizing a digital TX coil topology that is robust against the variation of distance and lateral

misalignment is proposed. Its radius can be programed to its optimal value for the maximum coil-to-coil efficiency for each position of the RX coil. A practical design methodology is proposed, and it is concluded that the digital TX coil consisting of two subcoils is an effective design and that the performance is not significantly improved by adding more subcoils. The optimal radius ratio of these two subcoils is 0.54. In the fabricated WPT prototype, the system efficiency is improved by the digital TX coil and reaches a maximum value of 48%. Compared with using a conventional TX coil with a constant radius, the system efficiency shows an absolute improvement of up to 7%.

REFERENCES

- [1] Z. Zhang, H. Pang, A. Georgiadis, and C. Cecati, "Wireless power transfer—An overview," *IEEE Trans. Ind. Electron.*, vol. 66, no. 2, pp. 1044–1058, Feb. 2019.
- [2] C.-G. Kim, D.-H. Seo, J.-S. You, J.-H. Park, and B. H. Cho, "Design of a contactless battery charger for cellular phone," *IEEE Trans. Ind. Electron.*, vol. 48, no. 6, pp. 1238–1247, Jun. 2001.
- [3] T. Campi, S. Cruciani, F. Palandrani, V. De Santis, A. Hirata, and M. Feliziani, "Wireless power transfer charging system for AIMDs and pacemakers," *IEEE Trans. Microw. Theory Techn.*, vol. 64, no. 2, pp. 633–642, Feb. 2016.
- [4] Q. Zhu, Y. Guo, L. Wang, C. Liao, and F. Li, "Improving the misalignment tolerance of wireless charging system by optimizing the compensate capacitor," *IEEE Trans. Ind. Electron.*, vol. 62, no. 8, pp. 4832–4836, Aug. 2015.
- [5] A. P. Sample, D. A. Meyer, and J. R. Smith, "Analysis, experimental results, and range adaptation of magnetically coupled resonators for wireless power transfer," *IEEE Trans. Ind. Electron.*, vol. 58, no. 2, pp. 544–554, Feb. 2011.
- [6] J. Park, Y. Tak, Y. Kim, Y. Kim, and S. Nam, "Investigation of adaptive matching methods for near-field wireless power transfer," *IEEE Trans. Antennas Propag.*, vol. 59, no. 5, pp. 1769–1773, May 2011.
- [7] T. C. Beh, M. Kato, T. Imura, S. Oh, and Y. Hori, "Automated impedance matching system for robust wireless power transfer via magnetic resonance coupling," *IEEE Trans. Ind. Electron.*, vol. 60, no. 9, pp. 3689–3698, Sep. 2013.
- [8] Y. Lim, H. Tang, S. Lim, and J. Park, "An adaptive impedance-matching network based on a novel capacitor matrix for wireless power transfer," *IEEE Trans. Power Electron.*, vol. 29, no. 8, pp. 4403–4413, Aug. 2014.
- [9] T. P. Duong and J.-W. Lee, "Experimental results of high-efficiency resonant coupling wireless power transfer using a variable coupling method," *IEEE Microw. Wireless Compon. Lett.*, vol. 21, no. 8, pp. 442–444, Aug. 2011.
- [10] J. Kim and J. Jeong, "Range-adaptive wireless power transfer using multiloop and tunable matching techniques," *IEEE Trans. Ind. Electron.*, vol. 62, no. 10, pp. 6233–6241, Oct. 2015.
- [11] G. Lee, B. H. Waters, Y. G. Shin, J. R. Smith, and W. S. Park, "A reconfigurable resonant coil for range adaptation wireless power transfer," *IEEE Trans. Microw. Theory Techn.*, vol. 64, no. 2, pp. 624–632, Feb. 2016.
- [12] J. L. Villa, J. Sallan, J. F. S. Osorio, and A. Llombart, "High-misalignment tolerant compensation topology for ICPT systems," *IEEE Trans. Ind. Electron.*, vol. 59, no. 2, pp. 945–951, Feb. 2012.
- [13] W. Li, H. Zhao, S. Q. Li, J. J. Deng, T. Kan, and C. C. Mi, "Integrated LCC compensation topology for wireless charger in electric and plug-in electric vehicles," *IEEE Trans. Ind. Electron.*, vol. 62, no. 7, pp. 4215–4225, Jul. 2015.
- [14] L. Zhao, D. J. Thrimawithana, and U. K. Madawala, "Hybrid bidirectional wireless EV charging system tolerant to pad misalignment," *IEEE Trans. Ind. Electron.*, vol. 64, no. 9, pp. 7079–7086, Sep. 2017.
- [15] T.-H. Kim, G.-H. Yun, W. Y. Lee, and J.-G. Yook, "Asymmetric coil structures for highly efficient wireless power transfer systems," *IEEE Trans. Microw. Theory Techn.*, vol. 66, no. 7, pp. 3443–3451, Jul. 2018.
- [16] B. H. Waters, B. J. Mahoney, G. Lee, and J. R. Smith, "Optimal coil size ratios for wireless power transfer applications," in *Proc. IEEE Int. Symp. Circuits Syst. (ISCAS)*, Jun. 2014, pp. 2045–2048.
- [17] J. Kim, D.-H. Kim, and Y.-J. Park, "Free-positioning wireless power transfer to multiple devices using a planar transmitting coil and switchable impedance matching networks," *IEEE Trans. Microw. Theory Techn.*, vol. 64, no. 11, pp. 3714–3722, Nov. 2016.

- [18] D. Liu, H. Hu, and S. V. Georgakopoulos, "Misalignment sensitivity of strongly coupled wireless power transfer systems," *IEEE Trans. Power Electron.*, vol. 32, no. 7, pp. 5509–5519, Jul. 2017.
- [19] F. Lu, H. Hofmann, J. Deng, and C. Mi, "Output power and efficiency sensitivity to circuit parameter variations in double-sided LCC-compensated wireless power transfer system," in *Proc. IEEE Appl. Power Electron. Conf. Expo. (APEC)*, Mar. 2015, pp. 507–601.
- [20] H. Qiu, Y. Narusue, Y. Kawahara, T. Sakurai, and M. Takamiya, "Digital coil: Transmitter coil with programmable radius for wireless powering robust against distance variation," in *Proc. IEEE Wireless Power Transf. Conf.*, Jun. 2018, pp. 1–4.
- [21] C. Zheng, H. Ma, J.-S. Lai, and L. Zhang, "Design considerations to reduce gap variation and misalignment effects for the inductive power transfer system," *IEEE Trans. Power Electron.*, vol. 30, no. 11, pp. 6108–6119, Nov. 2015.
- [22] K. Hata, T. Imura, and Y. Hori, "Simplified measuring method of kQ product for wireless power transfer via magnetic resonance coupling based on input impedance measurement," in *Proc. 43rd Annu. Conf. IEEE Ind. Electron. Soc. (IECON)*, Oct. 2017, pp. 6974–6979.
- [23] J. Kim and Y.-J. Park, "Approximate closed-form formula for calculating ohmic resistance in coils of parallel round wires with unequal pitches," *IEEE Trans. Ind. Electron.*, vol. 62, no. 6, pp. 3482–3489, Jun. 2015.
- [24] G. Smith, "The proximity effect in systems of parallel conductors and electrically small multirun loop antennas," Div. Eng. Appl. Phys., Harvard Univ., Cambridge, MA, USA, Tech. Rep. 624, 1971.
- [25] C. Akyel, S. I. Babic, and M.-M. Mahmoudi, "Mutual inductance calculation for non-coaxial circular air coils with parallel axes," *Prog. Electromagn. Res.*, vol. 91, pp. 287–301, Jan. 2009.
- [26] R. H. Good, "Elliptic integrals, the forgotten functions," *Eur. J. Phys.*, vol. 22, no. 2, pp. 119–126, Mar. 2001.
- [27] C. Nagai *et al.*, "Scaling law of coupling coefficient and coil size in wireless power transfer design via magnetic coupling," *Electr. Eng. Jpn.*, vol. 202, no. 4, pp. 21–30, Mar. 2018.
- [28] J. P. K. Sampath, A. Alphones, L. Y. Y. Kenneth, and D. M. Vilathgamuwa, "Analysis on normalized distance and scalability in designing wireless power transfer," in *Proc. IEEE PELS Workshop Emerg. Technol., Wireless Power (WoW)*, Jun. 2015, pp. 1–6.
- [29] *10 W Multi-Mode Wireless Power Amplifier EPC9511 Datasheet*, EPC, Chennai, India, 2016.
- [30] H. Qiu, Y. Narusue, Y. Kawahara, T. Sakurai, and M. Takamiya, "Distance detection system for digital transmitter coil achieving distance-variation-tolerant wireless power transfer," in *Proc. IEEE 15th Brazilian Power Electron. Conf., 5th IEEE Southern Power Electron. Conf. (COBEP/SPEC)*, Dec. 2019, pp. 830–835.



Hao Qiu (Member, IEEE) received the B.S. degree in materials science and the M.Eng. degree in electrical engineering from Nanjing University, Nanjing, China, in 2010 and 2013, and the Ph.D. degree in electrical engineering from The University of Tokyo, Tokyo, Japan, in 2016, respectively.

He has been a Researcher with The University of Tokyo. His research interests cover materials, devices, and circuits. His present focus is circuit design for wireless power transfer and wireless communication systems for IoT applications.

Dr. Qiu served as a Research Fellow with the Japan Society for the Promotion of Science from 2015 to 2017 and a Representative with the Japan Society of Applied Physics from 2016 and 2018. He received the 2016 IEEE Electron Devices Society (EDS) Japan Chapter Student Award and the 2017 Chinese Government Award for Outstanding Self-Finance Students Abroad.



Takayasu Sakurai (Fellow, IEEE) received the Ph.D. degree in electrical engineering from The University of Tokyo, Tokyo, Japan, in 1981.

In 1981, he joined Toshiba Corporation, Tokyo, where he designed CMOS DRAM, SRAM, and RISC processors, DSPs, and SoC Solutions. He has worked extensively on interconnect delay and capacitance modeling, known as the Sakurai model and the alpha power-law MOS model. From 1988 to 1990, he was a Visiting Researcher with the University of California at Berkeley, Berkeley, CA, USA, where he conducted research in the field of VLSI CAD. Since 1996, he has been a Professor with The University of Tokyo, Tokyo, where he is involved in low-power high-speed VLSI, memory design, interconnects, ubiquitous electronics, organic IC's, and large-area electronics. He is also a Domain Research Supervisor for nano-electronics area with the Japan Science and Technology Agency, Kawaguchi, Japan. He has filed more than 200 patents. He has authored or coauthored more than 600 technical publications, including 100 invited presentations and several books.

Dr. Sakurai is an IEICE Fellow. He was an Elected AdCom Member for the IEEE Solid-State Circuits Society and an IEEE CAS and SSCS Distinguished Lecturer. He was a recipient of the 2004 IEEE Takuo Sugano Award, the 2005 IEEE ICICDT Award, the 2005 P&I Patent of the Year Award, the 2009 IEICE Achievement Award, the IEEE Paul Rappaport Award in 2009 and 2010, respectively, the 2010 IEEE Donald O. Pederson Award in Solid-State Circuits, the 2010 IEICE Electronics Society Award, and four product awards. He served as the Conference Chair for the Symposium on VLSI Circuits and ICICDT, the Vice Chair for ASPDAC, the TPC Chair for the IEEE A-SSCC and the VLSI Symposium, an Executive Committee Member for ISLPED, and a Program Committee Member for the International Solid-State Circuits Conference (ISSCC), CICC, A-SSCC, DAC, ESSCIRC, ICCAD, ISLPED, and other international conferences. He is the Executive Committee Chair of the VLSI Symposia and a Steering Committee Chair of the IEEE A-SSCC. He delivered keynote speech at more than 50 conferences, including ISSCC, ESSCIRC, and ISLPED.



Makoto Takamiya (Senior Member, IEEE) received the B.S., M.S., and Ph.D. degrees in electronic engineering from The University of Tokyo, Tokyo, Japan, in 1995, 1997, and 2000, respectively.

In 2000, he joined NEC Corporation, Tokyo, where he was engaged in the circuit design of high-speed digital LSI's. In 2005, he joined The University of Tokyo, where he is currently a Professor with the Institute of Industrial Science. From 2013 to 2014, he was a Visiting Scholar with the University of California at Berkeley, Berkeley, CA,

USA. His research interests include the integrated power management circuits for wireless powering and energy harvesting for wearable and IoT applications and the digital gate driver IC for power electronics.

Dr. Takamiya is a member of the Technical Program Committee of the IEEE International Solid-State Circuits Conference (ISSCC). He received the IEEE Paul Rappaport Award in 2009 and 2010, respectively, and the Best Paper Award in the 2013 IEEE Wireless Power Transfer Conference. He served on the technical program committees of the IEEE Custom Integrated Circuits Conference from 2006 to 2011 and the IEEE Symposium on VLSI Circuits from 2009 to 2017. He is the Far East Regional Chair in ISSCC 2020. He is a Distinguished Lecturer of the IEEE Solid-State Circuits Society.